Original Article

Microvessels derived from hiPSCs are a novel source for angiogenesis and tissue regeneration

Journal of Tissue Engineering
Volume 13: 1–21

DOI: 10.1177/20417314221143240
journals.sagepub.com/home/tej
SAGE

Xin Gao#, Shixing Ma#, Xiaotao Xing#, Jian Yang, Xun Xu, Cheng Liang, Yejia Yu, Lei Liu, Li Liao and Weidong Tian

Abstract

The establishment of effective vascularization represents a key challenge in regenerative medicine. Adequate sources of vascular cells and intact vessel fragments have not yet been explored. We herein examined the potential application of microvessels induced from hiPSCs for rapid angiogenesis and tissue regeneration. Microvessels were generated from human pluripotent stem cells (iMVs) under a defined induction protocol and compared with human adipose tissue-derived microvessels (ad-MVs) to illustrate the similarity and differences of the alternative source. Then, the therapeutic effect of iMVs was detected by transplantation in vivo. The renal ischemia-reperfusion model and skin damage model were applied to explore the potential effect of vascular cells derived from iMVs (iMVs-VCs). Besides, the subcutaneous transplantation model and muscle injury model were established to explore the ability of iMVs for angiogenesis and tissue regeneration. The results revealed that iMVs had remarkable similarities to natural blood vessels in structure and cellular composition, and were potent for vascular formation and self-organization. The infusion of iMVs-VCs promoted tissue repair in the renal and skin damage model through direct contribution to the reconstruction of blood vessels and modulation of the immune microenvironment. Moreover, the transplantation of intact iMVs could form a massive perfused blood vessel and promote muscle regeneration at the early stage. The infusion of iMVs-VCs could facilitate the reconstruction and regeneration of blood vessels and modulation of the immune microenvironment to restore structures and functions of damaged tissues. Meanwhile, the intact iMVs could rapidly form perfused vessels and promote muscle regeneration. With the advantages of abundant sources and high angiogenesis potency, iMVs could be a candidate source for vascularization units for regenerative medicine.

Keywords

Angiogenesis, vascular cells, stem cells, vascular regeneration

Date received:: 12 July 2022; accepted: 18 November 2022

Introduction

Angiogenesis is an essential process in tissue repair and regeneration. Blood vessels supply oxygen and nutrients to ensure the survival and biological function of migrated or transplanted tissue cells.[1] The impact of vascularization on regenerative outcomes has been demonstrated.[2,3] Vascular instability and slow infiltration of vessels can prevent adequate vascularization, leading to graft failure.[4] Recently, emerging studies have demonstrated that engraftments containing vessel fragments efficiently promote cell survival and reconstitution of graft function.[5,6] Human adipose tissue-derived microvessels (ad-MVs) have represented a high angiogenic activity after their seeding on scaffolds and subsequent in vivo implantation.[5,7] Ad-MVs can rapidly

State Key Laboratory of Oral Diseases & National Clinical Research Center for Oral Diseases & Engineering Research Center of Oral Translational Medicine, Ministry of Education & National Engineering Laboratory for Oral Regenerative Medicine & Department of Oral and Maxillofacial Surgery, West China Hospital of Stomatology, Sichuan University, Chengdu, China

#means co-first author

Corresponding authors:
Li Liao, State Key Laboratory of Oral Disease, West China School of Stomatology, Sichuan University, 14# South Renmin Road, Chengdu, Sichuan 610018, China.
Email: lliao@scu.edu.cn

Lei Liu, Department of Oral and Maxillofacial Surgery, West China Hospital of Stomatology, Sichuan University, No.14, 3rd Section, Renmin South Road, Chengdu, Sichuan 610041, China.
Email: liulei@scu.edu.cn

interconnect and inosculate with the host vasculature within days of transplantation.[8] However, these approaches face the challenge of the limited source of adipose tissues. Finding out the optimal source of microvessels is crucial for rapid angiogenesis.

Several strategies, including 3-dimensional printing, microfluidic techniques, cell-laden microfibers, and cell infusion in piping systems, have been applied to fabricate microvessels.[9–11] However, two challenges limited the application of these strategies. First, is the lack of vascular cell sources. Studies showed that ad-MVs contain the major subgroups of vascular cells including endothelial cells and pericytes.[12] Due to the limit of cell proliferation in culture, it remains difficult to harvest large amounts of these vascular cells.[13] Second, is the lack of a well-defined culture system to support the regenerate functional microvessels. The suitable scaffold, cytokines, and culture system remain to be established.

Human induced pluripotent stem cells (hiPSCs) allow the harvesting of abundant cells of different lineages and generate microtissues with complicated cell components and structures. The discoveries that hiPSCs could differentiate into vascular cells in defined induction conditions were breakthroughs in microvessel engineering.[14–16] However, these protocols could not generate physiological vessel structures containing essential cell types. To facilitate the translation to the clinic, a more effective method should be developed to harvest different vascular cells for the generation of entire blood vessels. Recently, a pilot study by Wimmer et al. found that pluripotent stem cells could be induced to form self-organizing three-dimensional human blood microvessels.[17] These microvessels are initiated via mesoderm induction of hiPSCs aggregates and further differentiated into pericytes, and a few vascular smooth muscle cells (vSMCs), suggesting a possibility to generate microvessels via hiPSCs for tissue regeneration.[18]

In this study, we successfully generated microvessels from iPSCs (iMVs) and comprehensively compared iMVs with ad-MVs. Furthermore, we evaluated the angiogenic potential of vascular cells derived from iMVs (iMVs-VCs) in the animal model of renal ischemia-reperfusion (IR) and skin wounds. At last, we investigated the potential of iMVs for angiogenesis and tissue repair in the subcutaneous tissue regeneration model and muscle injury model. Our results demonstrated that iMVs had similar cell components, gene expression patterns, and structures to ad-MVs. The iMVs-VCs could directly be involved in the reconstruction and regeneration of blood vessels to facilitate tissue repair. Moreover, the transplantation of iMVs could regenerate perfused blood vessels in the early period and promote tissue regeneration. These findings suggest that iMVs could be applied for tissue repair and regeneration.

Methods

Animals

The animal experiments in this study were approved by the Experimental Animal Ethics Committee of West China Hospital of Stomatology, Sichuan University. Four-week-old male Balb/c nude mice were purchased from GemPhamatech Co, Ltd (Nanjing, China). All experimental procedures were performed under relevant guidelines and regulations.

Induction of hiPSCs to microvessels differentiation to generate vascular cells

Human-induced pluripotent stem cell line urine cell #1 (uc01) was kindly provided by Guangzhou Institutes of Biomedicine and Health, Chinese Academy of Science. The passage numbers of the UC cells used here ranged from 22 to 35. Undifferentiated hiPSCs were maintained in mTeSR medium (Stemcell Technologies, 85850) on Growth Factor Reduced Matrigel (Corning, 354320)—coated feeder-free plates. To coat the plates, 100 μL Matrigel from storage was added into 12 mL of prechilled, pure DMEM/F12 (Gibco, 21041025) to a 15-mL Falcon tube on ice. The prechilled six well plates were added 1 mL cold medium per well for 30 min at 37°C.

Protocol for blood vessel organoid generation was as described previously.[18] Briefly, for differentiation, hiPSCs were dissociated by 0.5 mM EDTA (Gibco, AM9260G) for 5 min and resuspended in 3 mL differentiation media (DMEM: F12 medium,12660012, 20% KOSR, 10828010, Glutamax, 35050079, NEAA, 1030021; all from Gibco) including 50 μM Y-27632 (Selleck, S6390). A total of 1×10^6 cells were plated into the ultra-low attachment surface six well plate (Corning, 3471) and incubated the cells for at least 1d until the cell aggregates with smooth borders (50–100 μM diameter). Then, cell aggregates were treated with 12 μM CHIR99021 (Selleck, S2924) and BMP-4 (30 ng/mL, Peprotech) on days 3–6 to induce mesoderm, followed by VEGF-A (100 ng/mL, Peprotech, 120-05) and 2 μM forskolin (Selleck, S2449) treatment to trigger vascular development on days 7–9. Gentle treatment of aggregates was important. Always collect aggregates by gravitation. The resulting cell aggregates were embedded in a collagen I-Matrigel (3:1) matrix and overlaid with prewarmed StemPro-34 SFM (Gibco, 10639011) complete medium including 15% FBS, VEGF-A (100 ng/mL, Peprotech, 100-20), and FGF-2 (100 ng/mL, Peprotech, 100-26) for at least 5 days. A full six-well plate of aggregates was embedded in an entire 12-well plate, corresponding to 40–60 aggregates per well.

After vascular network formation, microvessels were extracted from gels by 1 mL needles, washed three times in PBS, and dissociated in Accutase (Stemcell Technologies,

07920) containing 0.2 U μL^{-1} Dnase I (Roche, 10104159001) for 45 min at 37°C, followed by filtering through 40 μm diameter strainers (Corning, 431750) to create iMVs-VCs suspension. Add an equal volume of PBS containing 2% FBS to stop the digestion. Cell viability was assessed by Trypan blue staining (Gibco, 15250016) and counted using an automatic cell counter (Countess, ThermoFisher).

Flow cytometric analysis

Flow cytometric analysis was conducted to detect the major cell populations presented in iMVs-VCs. Microvessels were dissociated into single cells according to the above method. The cell mixture was washed and resuspended in 2%FBS/PBS containing the following antibodies for 30 min at 4°C: Isotype control (Thermo, PA5-33198), PE Mouse anti-Human CD31 (Biolegend, 303105, 5 μL/test), and PE Mouse anti-Human CD140b (BD, 558821, 5 μL/test). Then, cells were washed three times and resuspended in 2%FBS/PBS for analysis by an Accuri C6 flow cytometer (BD). The control group was used to exclude debris and doublets and yield the total cell population. Gating the negative cells was critical in this assay. Subsequently, CD31-positive and CD140b-positive cells were gated according to the isotype control. The data were analyzed using FlowJo V10 software.

Tube formation assay

The tube formation assay was used to investigate the angiogenic activity of iMVs-VCs. First, allow the Matrigel (Corning, 354234) to thaw at 4°C, and coated u-Slide (iBide, 81506) with 10 μL per well of Matrigel. Let the plates sit at room temperature for at least 15 min to allow gelling of the Matrigel. Then, plate 50 μL of iMVs-VCs, which contained 8000–10,000 cells, into each Matrigel-coated well. The dish was incubated at 37°C for at least 6 h. Pictures were taken at 12 and 24 h to observe the tube structures.

Isolation of ad-MVs

Human adipose tissues were obtained from patients conducting cosmetic liposuction at Sichuan Huamei Zixin Medical Aesthetic Hospital. The ad-MVs were isolated as described previously.[19] Briefly, wash 5 mL adipose tissues with 15 mL α -MEM containing 2% penicillin-streptomycin. After washing, the tissues were cut up with scissors. Centrifuge the tissues at 300*g* for 5 min and aspirate the medium. The 5 mL adipose tissues were digested for 15 min with 10 mL collagenase I (1 mg/mL, Sigma, SCR103) at 37°C. The digestion was neutralized with an equal volume of α—MEM supplemented with 20% FBS. Aspirate the fat supernatant. The remaining suspension was filtered using a 500 μm strainer (pluriSelect, 435000199) to remove undigested adipose tissues and a 20 μm strainer (pluriSelect, 435000199) to harvest ad-MVs. Then, ad-MVs were washed from the 20 μm strainers and collected by centrifugation at 5 min, 600*g*.

Library construction and RNA-sequencing

Three ad-MVs samples, as the control group, and three iMVs-VCs samples were separately treated with TRIzol Reagent (Invitrogen, 10296028). RNA was collected from each sample according to the manufacturer's instructions and genomic DNA was removed using DNase I (TaKara, 2270A). Then RNA quality was determined by 2100 BIoanalyser (Agilent) and quantified using the ND-2000 (NanoDrop Technologies). Only a high-quality RNA sample (OD260/280 = 1.8–2.2, OD260/230 ⩾ 2.0, RIN ⩾ 6.5, 28S:18S ⩾ 1.0, >1 μg) was used to construct the sequencing library. RNA-seq transcriptome library was prepared following the TruSeq™ RNA sample preparation Kit from Illumina using 1 μg of total RNA. Shortly, messenger RNA was isolated according to the polyA selection method by oligo(dT) beads, and the RNA was fragmented and reverse-transcribed into single-stranded cDNA. Then, double-stranded cDNA was synthesized using a SuperScript double-stranded cDNA synthesis kit (Invitrogen) with random hexamer primers (Illumina). After PCR amplification and purification, the library was paired-end sequenced at Shanghai Majorbio Bio-pharm Technology Co., Ltd using the Illumina HiSeq Xten/NovaSeq 6000 sequencer (2 × 150 bp read length).

Expression analysis

The expression level of each transcript was calculated according to the transcripts per million reads (TPM) method. RSEM (http://deweylab.biostat.wisc.edu/rsem/) was used to quantify gene abundances. Essentially, differential expression analysis was performed using the DESeq2 with Q value ⩽ 0.05, DEGs with |log2FC|>1 were considered to be significantly differentially expressed genes). In addition, functional-enrichment analyses including GO and KEGG were performed to identify which DEGs were significantly enriched in GO terms and metabolic pathways at Bonferroni-corrected p-value ⩽ 0.05 compared with the whole-transcriptome background. GO functional enrichment, KEGG pathway analysis, GSEA analysis were carried out by Goatools (https://github.com/tanghaibao/Goatools) and KOBAS (http://kobas.cbi.pku.edu.cn/home.do).

Renal ischemia-reperfusion injury model

The renal ischemia-reperfusion (IR) injury model was performed as previously described with modifications.[20] In brief, nude mice were anesthetized by an intraperitoneal

injection of pentobarbital (10%, Sigma, 57330), and unilateral/bilateral renal pedicle occlusions were induced by vascular clamping for 45 min. Ischemia was confirmed by the color change of the kidney. With the removal of the clamp, the color of the kidney quickly changed from purple-black to bright red, which indicated proper reperfusion. After the layered suture, the iMVs-VCs (2×10^5 cells/mouse) in 0.1 mL PBS were injected by tail intravenous injection (iMVs-VCs group). Meanwhile, mice injected with 0.1 mL PBS (as vehicle control) as the IR group, and normal mice without any treatment were the normal group. At 5- or 30-days post-injection, the mice were sacrificed. The kidneys were collected. The blood samples from mice with bilateral injuries were collected on day 5.

Skin damage model

Nude mice were anesthetized by an intraperitoneal injection of pentobarbital (10%, Sigma), and then a full-thickness wound with a length of 2 cm on both sides of the mouse's back. After aligning the suture, the iMVs-VCs (2×10^5 cells/mouse) in 0.1 mL PBS were injected intracutaneously on the left side (VCs side) and 0.1 mL PBS was injected on the right side (PBS side) from the incision about 1 cm. Wounds were collected at 3- or 30 days for analysis.

Angiogenesis in vivo assay

To explore the angiogenic ability of iMVs in vivo, a custom-designed silicone tube was used to load 4–6 iMVs in 100 μL collagen I-Matrigel (3:1) matrix and implanted into the back of nude mice. The silicone tube containing collagen I-Matrigel (3:1) matrix only was used as the control group. Samples were collected at 2 and 4 weeks.

Muscle injury model

BALB/c-Nude mice (4 weeks of age; approx. 20g; GemPharmatech, Nanjing; China) were used for the muscle injury model. Unilateral muscle defects measuring 1.5 cm in length, 0.5 cm in width, and 0.5 cm in height were created by removing the middle portion of the tibialis anterior muscle of recipient mice. Skin and fascia were separated from the underlying muscle using blunt dissection. The muscle was excised by two blades fixed at a 0.5 cm distance. Constructs were tightly placed into the defect site. The constructs were divided into three groups: collagen I-Matrigel (3:1) matrix as the control group, collagen I-Matrigel (3:1) matrix containing 1×10^5 endothelial cells as the cell group, and collagen I-Matrigel (3:1) matrix containing 2–3 iMVs as the organoid group. The wound was closed in layers. At 30-days post-surgery, the mice were sacrificed. The middle portion of the tibialis anterior muscles was collected.

Histologic and immunofluorescence analysis

Frozen sections of formalin-fixed tissues (7 μm thick) were stained with hematoxylin and eosin (HE), Periodic acid Schiff (PAS), and Masson trichrome according to the manufacturer's recommended protocols to assess the histological injury, kidney tubular necrosis, and fibrosis. Immunofluorescence staining of primary antibodies was performed at 4°C overnight and labeled with secondary antigens for 30 min at 37°C. Nuclei were marked with 4′ 6-diamidino-2-phenylindole (DAPI) for 5 min at room temperature. The primary antibodies of CD31 (Abcam, ab24590, 1:1000), CD140b (Zen, 345674, 1:100), and α-SMA (Abcam, ab5694, 1:100) were used to label vascular cells. Primary antibodies of CD163 (Abcam, ab182422, 1:200), and CD68 (Abcam, ab201340, 1:1000) were used to label macrophages. Human-derived cells were identified with human mitochondria (Abcam, ab92824, 1:800) and STEM101 (Takara, Y40400, 1:50). Regenerated myofibers were indicated by Myosin IIa antibody (CST, 3403, 1:50). The secondary antibodies of Alexa Fluor 488-conjugated goat anti-mouse (Invitrogen, A11001, 1:400) and Alexa Fluor 555-conjugated goat anti-rabbit (Invitrogen, A21428, 1:400) were used. Each group selected 4–6 random fields of view for analysis.

Biodistribution of the iMVs-VCs in vivo

iMVs-VCs (2×10^5 cells/mouse) were labeled with fluorescent lipophilic tracer DiR (Invitrogen) according to the manufacturer's instructions. Briefly, the iMVs-VCs were incubated with labeling solutions for 30 min at 37°C. After labeling, the cells were spun, rinsed, and resuspended in 0.1 mL PBS. And then, the labeled iMVs-VCs were injected intravenously or intracutaneously into animal models. The biodistribution of the iMVs-VCs was imaged using the IVIS Spectrum (PerkinElmer) for the first 3 days.

Blood urea nitrogen analysis

Blood samples were collected to test the kidney functional biomarker blood urea nitrogen (BUN, BOXBIO) according to the manufacturer's instructions.

Western blot analysis

The total proteins were extracted by RIPA lysis buffer containing protease inhibitors PMSF (100:1) (Millipore, USA), and BCA Protein Assay Kit (Bio-Rad, USA) was applied to quantify the proteins. 25 μg total proteins were loaded into 12% or 10% sodium dodecyl sulfate-polyacrylamide gel for electrophoresis to separate proteins of different molecular. Then, proteins were transferred onto blocked polyvinylidene difluoride (PVDF) membranes (Millipore, USA) at room temperature, and incubated

with primary antibodies: CD146 (Zen, 380835, 1:1000), VE-Cadherin (Abcam, ab33168, 1:1000), VWF (Abcam, ab154193, 1:1000) and β-actin (Zen,380624, 1:5000) at 4°C overnight. After washing, the membranes were incubated with appropriate horseradish peroxidase-conjugated secondary antibodies (Zen,1:5000) at room temperature for 60 min, and visualized by a western lightning chemiluminescence detection kit (PerkinElmer, N0775330). Relative signal intensities were determined using the ImageJ software.

Statistical analysis

We performed statistical analyses with GraphPad Prism 9(GraphPad Software, 9.1.1, California USA). For the quantification of the images, four different fields of images are selected for statistics. One-way analysis of variance, a two-tailed unpaired t-test was utilized to identify significant differences, which were accepted when the *p*-value was less than 0.05.

Data availability

The data that support the findings of this study are available from the corresponding author upon reasonable request.

Results

Generation of iMVs from hiPSCs

To generate iMVs, hiPSCs were induced with sequential cocktails of small molecules and growth factors First, hiPSCs were treated with ROCK inhibitor to induce the autonomous formation of aggregates. Stimulation of CHIR99021 and BMP-4 induced mesodermal differentiation of iPSCs. VEGF-A and FGF-2 were then used for vascular lineage induction. Subsequently, the cell aggregates were embedded in collagen I-Matrigel gels, which provide a 3D scaffold to facilitate the vessel sprouting (Figure 1(a)).[21] During vessel sprouting, cells gradually migrated outward from the aggregates and formed microvessel-like structures (Figure 1(b)). The immunofluorescence analysis of CD31 and CD 140b showed that $CD31^+$ endothelial cells and $CD140b^+$ pericytes were located around the wall of microvessels and formed a 3-dimensional network structure. (Figure 1(c) and (d)). Taken together, we successfully generated iMVs from hiPSCs.

Comparisons between iMVs and ad-MVs

To further evaluate the resemblances between iMVs and natural blood vessels, we compared the iMVs with as-MVs. As shown in Figure 2(a), immunofluorescence staining revealed a microvessel-like luminal structure with tight interaction between $CD140b^+$ pericytes and $CD31^+$ ECs, which was very similar to natural microvessels derived from adipose tissues.

To gain insight into the identity of iMVs, RNA-seq was conducted to compare gene expression between iMVs and ad-MVs. The Venn diagram showed that the iMVs expressed 16,530 genes, while the ad-MVs expressed 17,519 genes (Figure 2(b)). A total of 14,366 (72.99%) genes were co-expressed in iMVs and ad-MVs. There were 2164 genes (13.09%) only expressed in the iMVs and 3153 genes (18.00%) only expressed in the ad-MVs. The composition of the transcriptome is mostly common. Furthermore, a correlation analysis was performed to reveal the relevance between iMVs and ad-MVs from the statistical level. The average of Spearman's rank correlation coefficient between the two groups was 0.795, suggesting that iMVs and ad-MVs were genetically similar (Figure 2(c)).

We then compared prototypic marker genes of ECs, pericytes, and hiPSCs in two groups. The heatmap showed that both iMVs and ad-MVs expressed EC markers (PECAM1, ICAM2, and PTPRB) and pericytes markers (PDGFRB, ACTA2, and MYH11), albeit the slight difference in levels of expression (Figure 2(d)). It should be mentioned that the marker genes of hiPSCs could rarely be detected in iMVs (Figure 2(d)), suggesting the high efficiency of angiogenic differentiation. Western blot was also performed to show the maturation of iMVs. Similar to ad-MVs, iMVs expressed VE-Cadherin, CD146, and less VWF, which indicated the maturation of ECs and pericytes in iMVs (Figure 2(e)). Although the quantification of VE-Cadherin and VWF was statistically significant, the expression difference between the two groups was less than one-fold, suggesting the similarity.

To confirm the vascular functions of iMVs, GO analysis was employed. Figure 2(f) presented that the genes expressed in iMVs were involved not only in angiogenesis but also in the regulation of blood pressure, coagulation, and vascular permeability. Moreover, genes involved in the wound healing pathways, as well as organ development pathways, were enriched in iMVs.

We further identified the pathways of iMVs involved in angiogenesis and healing. As shown in Figure 2(g), the iMVs could activate the homology direct repair and involve the transcriptional regulation of stem cells. Meanwhile, the iMVs played a positive role in regulating the migration of endothelial and epidermal cells. In addition to regulating muscle organization, the iMVs also promoted epithelial keratinization. Taken together, these results revealed that iMVs shared fairly similar genetic signatures with natural microvessels and possessed potential capacities for angiogenesis and tissue regeneration.

Identification of VCs from iMVs

To further clarify the cellular composition of iMVs, immunofluorescence and flow cytometry assays were performed to detect ECs, pericytes, and vSMCs in the cells isolated from iMVs. Immunofluorescence staining revealed that

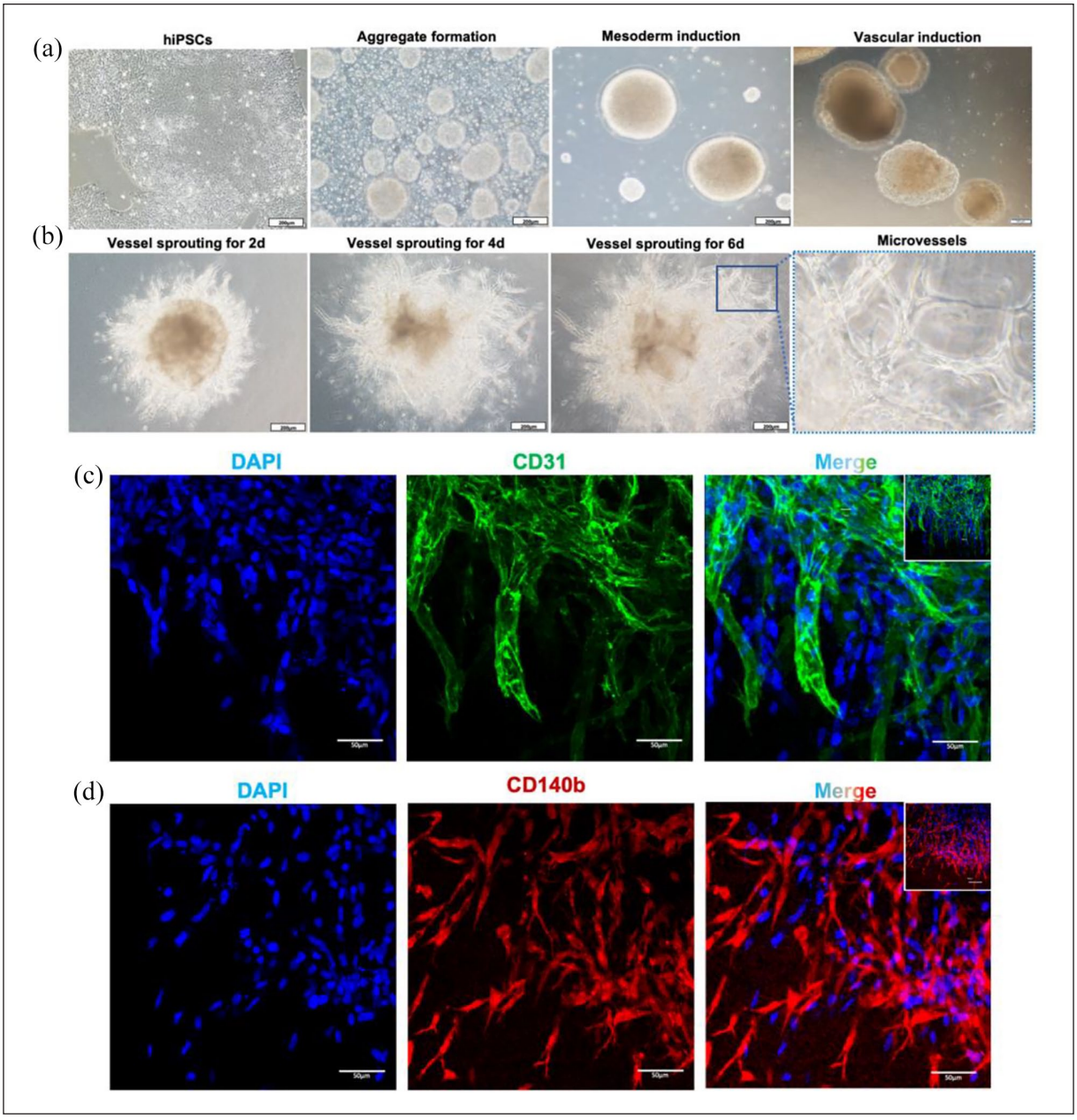

Figure 1. Generation of iMVs. (a) The iMVs were initiated from hiPSCs aggregates to mesodermal induction and further differentiated into the vascular lineage. Scale bar, 200 μm. (b) By embedding the aggregates into the collagen I-Matrigel matrix, microvessels sprouted from the aggregates and formed vascular networks. Scale bar, 200 μm. The right of the image is a magnification of the region within the blue box. (c) Immunofluorescence of microvessels on day 15 showed luminal structures formed by ECs expressing CD31 (in green). Scale bar, 50 μm. (d) Immunofluorescence of microvessels on day 15 showed a network structure formed by pericytes expressing CD140b (in red). Scale bar, 50 μm.

$CD140b^+$ pericytes and $CD31^+$ ECs accounted for a large proportion of the cells isolated from iMVs, while only a few cells expressed α-SMA (Figure 3(a)–(c)). Meanwhile, flow cytometry defined that 64.4% of iMVs-VCs expressed pericyte markers CD140b. 22.9% of iMVs-VCs expressed CD31 (Figure 3(d)).

We further explored the potency of iMVs-VCs for angiogenesis in vitro through tube formation assay. iMVs-VCs were digested from iMVs into single-cell suspension and then seeded on Matrigel. After 12 h, the iMVs-VCs formed a complex cell-cell network with close contact between ECs and pericytes (Figure 3(f) and (h)). Notably, the iMVs-VCs re-self-organized into cell aggregates after 24 h (Figure 3(g) and (i)). Recent data had indicated that cell aggregates could enhance cellular retention and angiogenic activity after transplantation.[22] The ability of iMVs-VCs in

self-organization, which involved embryonic development, regeneration, and formation of complex structures,[23] suggests the advantages of iMVs-VCs in tissue regeneration.

Taken together, these findings revealed the excellent angiogenesis and self-organization capabilities of iMVs-VCs.

Treatment effects of the iMVs-VCs on IR-induced injury in mice

To explore whether iMVs-VCs had therapeutic effects, we established a mouse model of renal ischemia-reperfusion

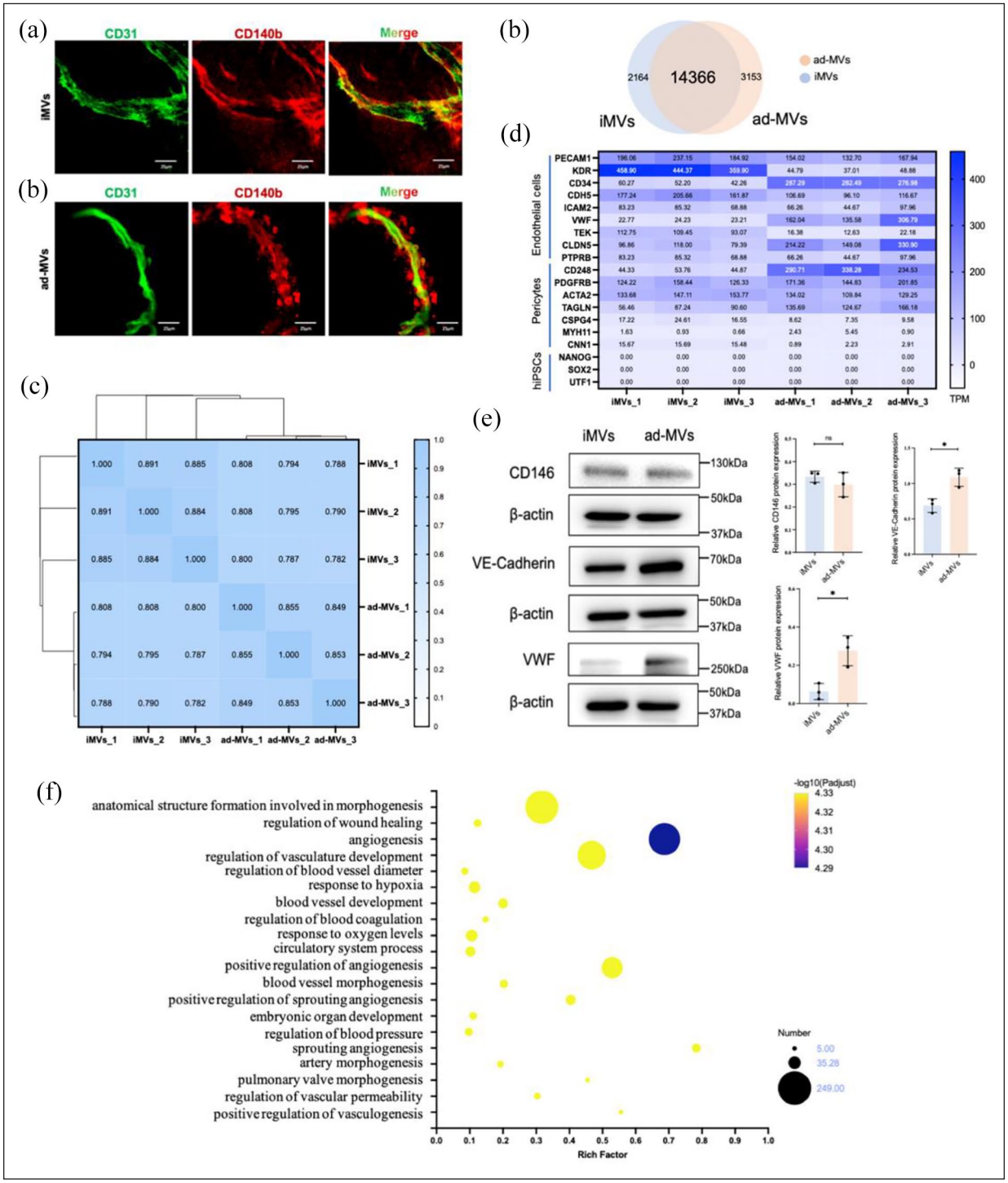

Figure 2. *(Continued)*

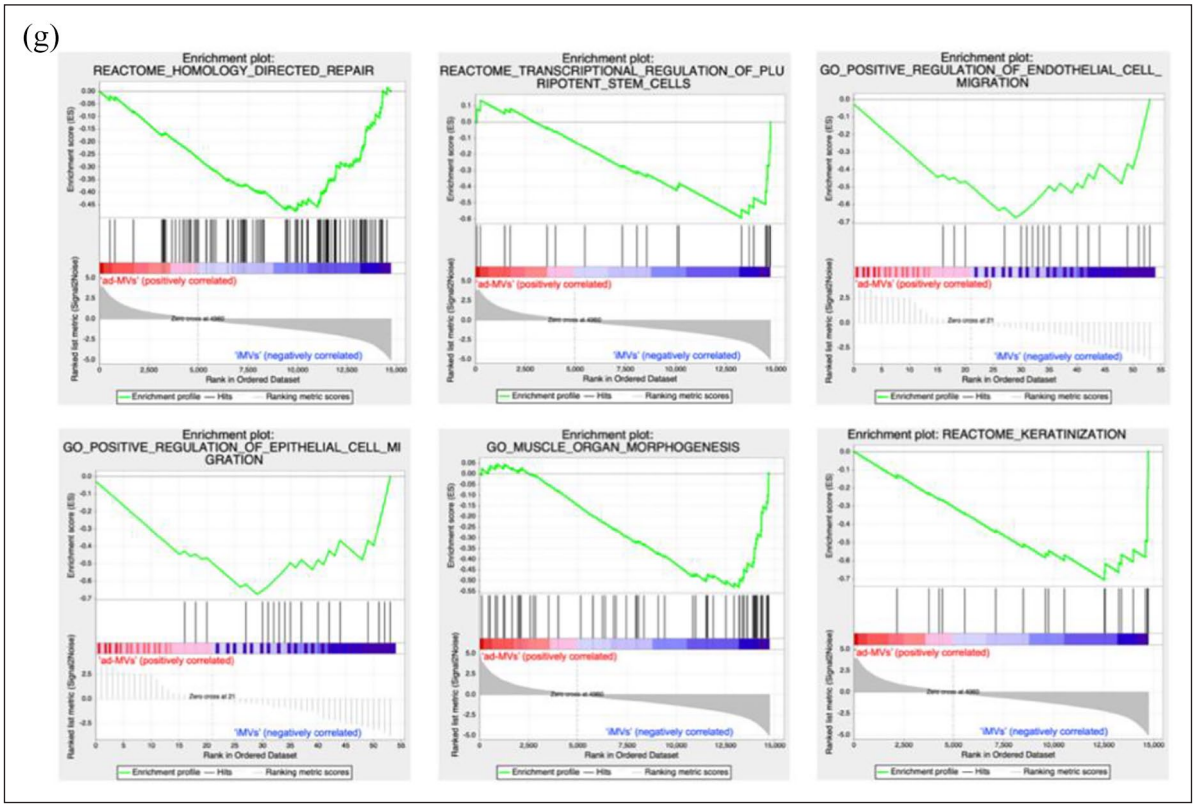

Figure 2. Comparisons between iMVs and ad-MVs. (a) Immunofluorescence analysis of iMVs and ad-MVs showed similar luminal structures surrounded by ECs (CD31 in green) and pericytes (CD140b in red). Scale bar, 100 μm. (b) Venn diagram revealed the shared and differential genes between the iMVs and ad-MVs groups. (c) Correlation analysis between iMVs and ad-MVs groups by Spearman. $0.8 < \rho < 1.0$ means significantly strong correlation; $0.6 < \rho < 0.8$ means strong correlation. (d) The marker genes of ECs, pericytes, and hiPSCs in iMVs and ad-MVs groups. TPM values of the above genes were summarized from transcripts. (e) The expressions of CD146, VE-Cadherin, and VWF protein in iMVs and ad-MVs were detected by western blot analysis. Data were shown as mean ± SD of three independent experiments, ns indicates no significance, $^{*}p < 0.05$, $^{**}p < 0.01$. (f) Go enrichment analysis for angiogenic genes in iMVs groups. The horizontal axis represented the ratio of the rich factor. The size of the dot indicated the number of genes in the pathway, and the color of the dot corresponded to a different -log10 (Padjust value), *p*-value corrected by the False Discovery Rate (FDR) method. (g) GSEA analysis revealed that compared with ad-MVs, iMVs-VCs positively regulated migration of ECs and epithelial cells, involved in homology-directed repair, regulation of stem cells, muscle morphogenesis, and promoted keratinization. The upper curve of the graph represents the dynamic enrichment score (ES) value, and the highest point represents the ES value of this gene set. The middle part of the figure represents the sorted sequence of the hybridization data, and the vertical lines represent the genes in the chip dataset appearing in this gene set. The lower curve in the figure shows the sorted values. $p < 0.01$.

(IR) injury, which induces sustained vascular damage. Transplantation of endothelial cells has been demonstrated to accelerate the repair of ischemia-reperfusion injury by attenuating endothelial damage.[24] Therefore, we administrated the iMVs-VCs intravenously into the IR mouse model 45 min after IR surgery (Figure 4(a)). Five days after surgery, the ischemic condition of the kidneys was alleviated in the iMVs-VCs treatment group (Figure 4(b)). Treatment of iMVs-VCs obviously decreased the blood urea nitrogen (BUN), a marker of glomerular filtration function to a level slightly higher than that of the normal group. HE staining showed administration of iMVs-VCs alleviated the disorganized structures, dilation of renal tubules, and atrophy of glomeruli of renal cortex at 5 days post-IR. (Figure 4(d)). Similarly, PAS staining revealed that the number of damaged tubules was reduced in the iMVs-VCs group compared with the IR group (Figure 4(e) and (f)). Moreover, Masson trichrome staining confirmed that the interstitial fibrosis area in the iMVs-VCs group was less than that in the IR group (Figure 4(g) and (h)). These results indicated that iMVs-VCs could preserve the structures of the kidney in the early stage of IR injury.

To investigate the long-term effects of iMVs-VCs on kidneys, renal samples were collected 30 days after IR surgery. There was no apparent difference in the color of the kidneys in each group (Figure 4(b)). HE staining showed ischemic necrosis in the IR group, while no obvious structural changes were observed in normal and iMVs-VCs groups (Figure 4(i)). Consistent with the results of 5 days after surgery, treatment of iMVs-VCs reduced the number

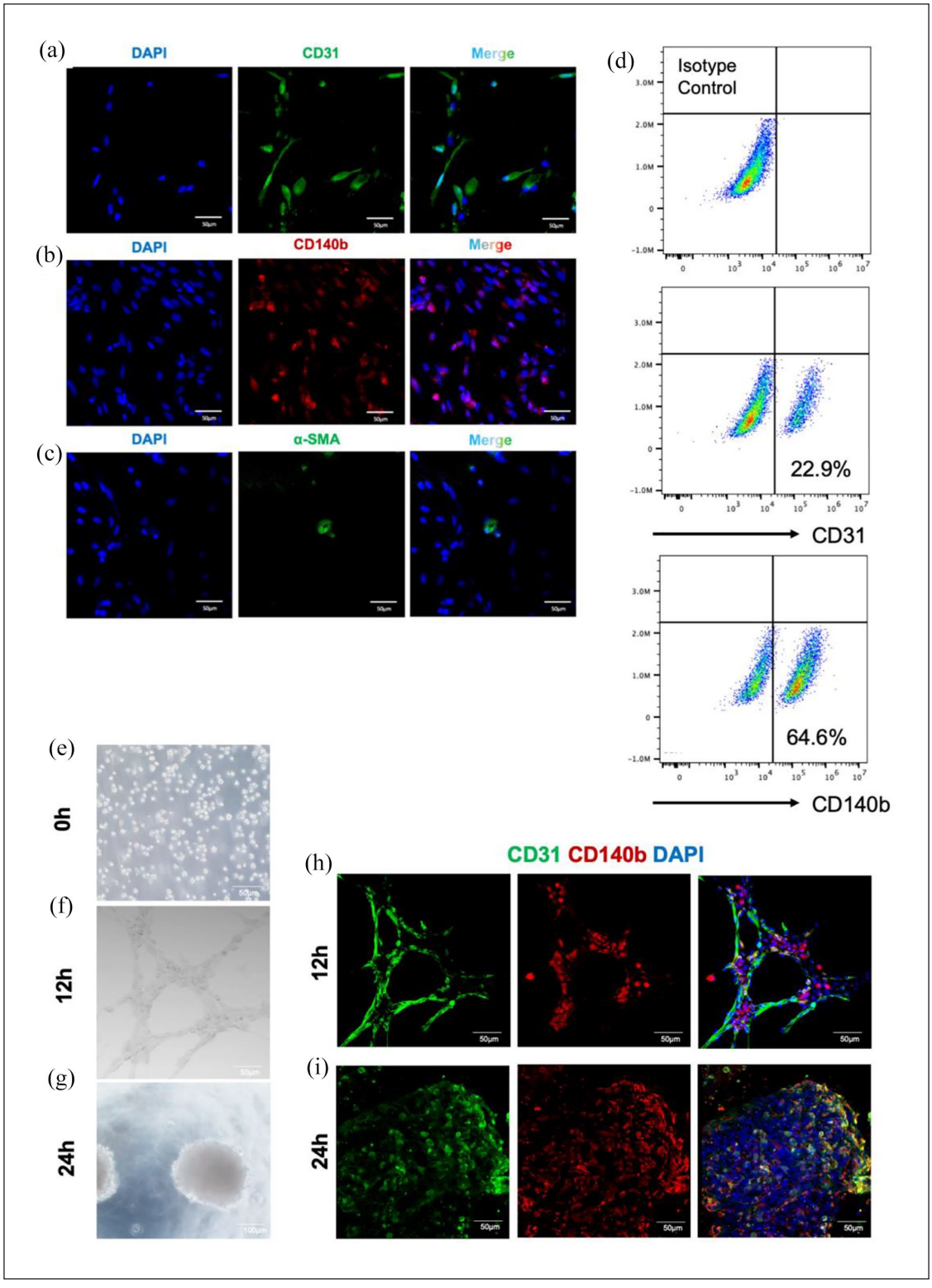

Figure 3. Identification of VCs from iMVs. (a–c) Immunofluorescence staining indicated ECs ($CD31^+$ in green), pericytes ($CD140b^+$ in red), and vSMCs (α-SMA^+ in green) in dissociated iMVs. Scale bar, 50 μm. (d) Flow cytometric analysis for the proportion of vascular cells. CD31 as a surface marker of ECs; CD140b as a surface marker of pericytes. (e–g) Images for tube formation analysis at three different times. After 12 h of seeding, the iMVs-VCs formed a cell-cell network; and 24 h later, the iMVs-VCs self-organized into aggregates. Scale bar, 100 μm. (h) Immunofluorescence of sprouting network showed the interaction between ECs (CD31 in green) and pericytes (CD140b in red) at 12 h. Scale bar, 100 μm. (i) Immunofluorescence of aggregates at 24 h indicated self-organization of ECs (CD31 in green) and pericytes (CD140b in red). Scale bar, 100 μm.

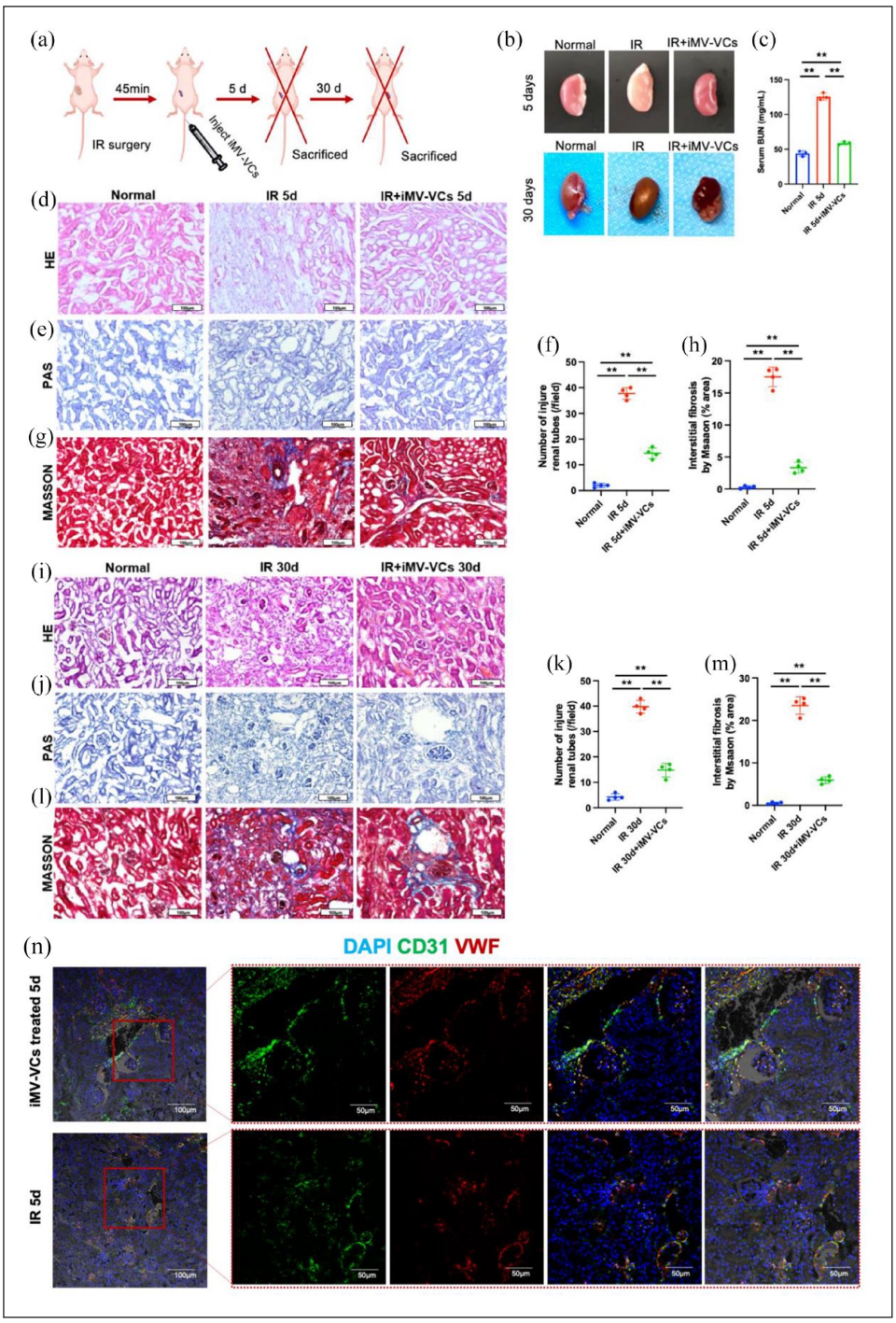

Figure 4. Therapeutic effects of iMVs-VCs on renal IR-induced injury in mice. (a) Experiment schematic. The renal IR-induced injury model was established. After the surgery, the iMVs-VCs were injected intravenously. At 5- or 30-days post-injection, the mice were sacrificed for sample collection. (b) Pictures of kidneys in different groups on 5- and 30-day. (c) Serum BUN test indicated that the iMVs-VCs protected the filtration function of the kidney after IR-induced injury. (d) HE staining was performed to reveal morphological changes in different groups. The administration of iMVs-VCs protected physiological structures against IR-induced injury on day 5. Scale bar, 100 μm. (e) PAS staining was performed to evaluate renal tubular injury by calculating tubules with dilation swelling or epithelial cell brush border loss. Scale bar, 100 μm. (f) Statistical values of tubular injury in different groups on day 5. (g) Masson staining indicated extracellular fibrotic collagen deposition in the renal interstitium. Scale bar, 100 μm. (h) Statistical values of collagen area in different groups on day 5. (i) After 30 days of treatment, HE staining was performed to reveal structural restoration. Scale bar, 100 μm. (j and k) PAS staining was performed to evaluate renal tubular injury on day 30. Scale bar, 100 μm. (l and m) Masson staining represented fibrosis in the renal interstitium during the repair. Scale bar, 100 μm. (n) Immunofluorescence of renal sections revealed the angiogenic capacity of iMVs-VCs by staining ECs (CD31 in green, VWF in red) on day 5. Scale bar, 100, 50 μm. Data were presented as the mean ± SD, $n = 3$–4/group, $^{*}p < 0.05$, $^{**}p < 0.01$.

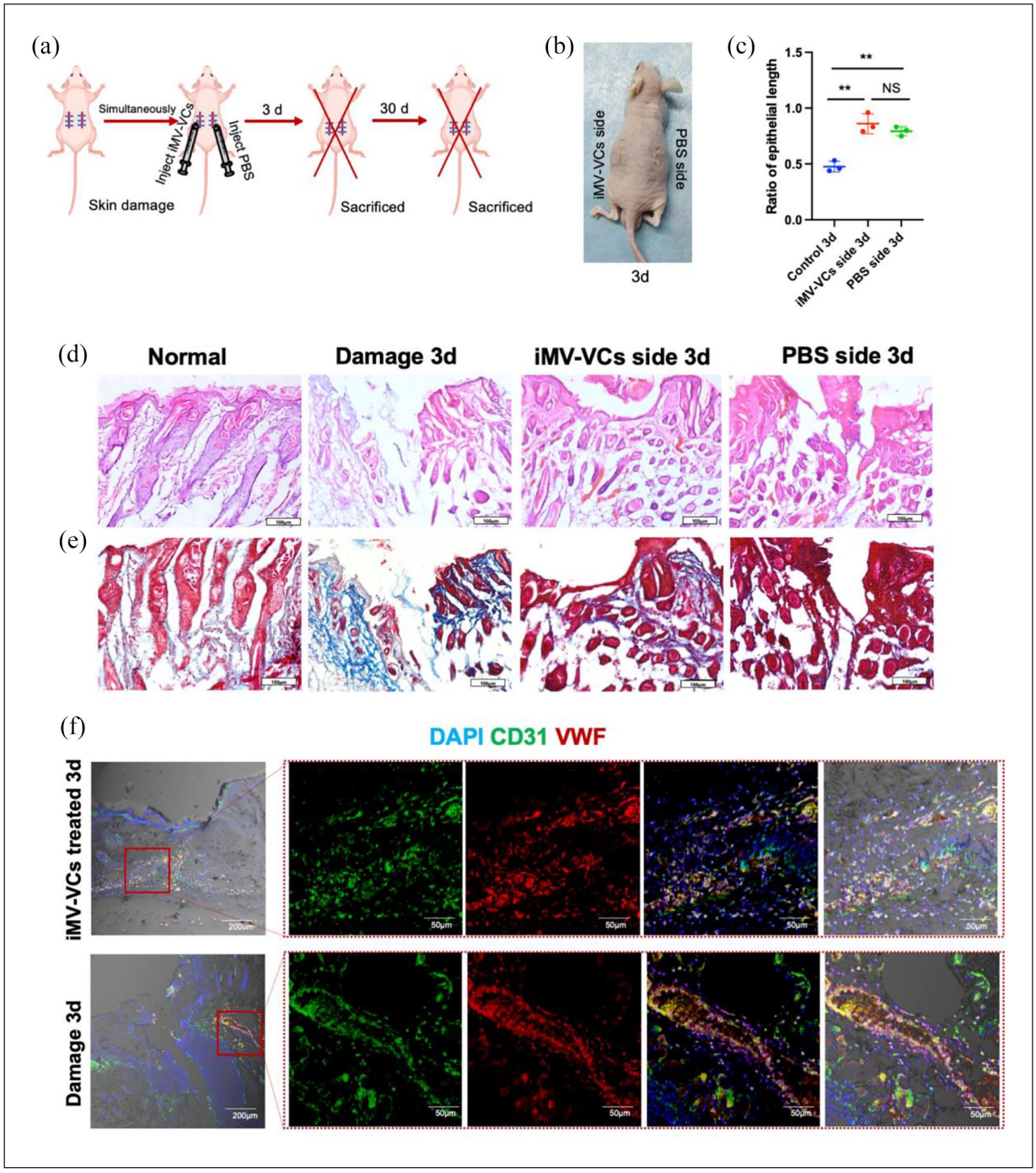

Figure 5. Therapeutic effects of iMVs-VCs on skin damage. (a) Experiment schematic. The skin damage model was established. After the surgery, the iMVs-VCs were injected intracutaneously. The mice were sacrificed for sample collection on day 3 and 30. (b) Pictures of skin on day 3 post-surgery. (c) Quantification of the length of regenerated epidermal tongue in different groups. (d) HE staining was performed to reveal pathological conditions of skin healing in different groups. Scale bar, 100 μm. (e) Masson staining indicated extracellular fibrotic collagen deposition in the damaged area. Scale bar, 100 μm. (f) Immunofluorescence of wound edges indicated the angiogenic capacity of iMVs-VCs by staining ECs (CD31 in green, VWF in red) on day 3. Scale bar, 200, 50 μm. Data are presented as the mean ± SD, $n = 3$/group, $^{*}p < 0.05$, $^{**}p < 0.01$.

of damaged tubules (Figure 4(j) and (k)) and attenuated the fibrosis (Figure 4(l) and (m)) after 30 days.

The angiogenic ability of iMVs-VCs was also detected by staining renal vessels after treatment for 5 days. Co-staining of CD31 and VWF were clearly observed in the renal glomerulus of iMVs-VCs groups, and many co-stained cells accumulated around the perfused vessels. However, the fluorescence intensity of glomerulus was

very low in the untreated group, although co-stained vessels were presented (Figure 4(n)). Taken together, the administration of iMVs-VCs could restore renal functions, inhibit interstitial fibrosis, and positively regulate angiogenesis.

iMVs-VCs promote the healing of skin wound

Rapid regeneration and reconstruction of blood vessels can stimulate wound healing.[25] To further evaluate the therapeutic effect of iMVs-VCs, a mice model of full-thickness skin wounds was established. iMVs-VCs were injected intracutaneously into the wound on one side (iMVs-VCs side) of the back of nude mice, and PBS was injected into the other side (PBS side). Nude mice with skin wounds on both sides untreated for spontaneous healing served as the blank control (damage group) (Figure 5(a)). After 3 days after surgery, both iMVs-VCs and PBS sides achieved skin healing (Figure 5(b)). HE and Masson trichrome staining were performed to assess the healing pathology of wounds treated by iMVs-VCs. As shown in Figure 5(c) to (e), unlike the damage group which exhibited a rare well-structured neoepidermis, complete skin repair was observed on the iMVs-VCs side on day 3. It should be noted that the PBS side also healed better than the damage group. There was no significant difference in the epithelial length between the iMVs-VCs and PBS sides (Figure 5(c)), suggesting that the locally transplanted iMVs-VCs could promote repair of the distant wound sites. We then observed the angiogenesis in damage and iMVs-VCs treated groups. The edges of the wound exhibited a large number of blood vessels (stained with VWF and CD31) in iMVs-VCs treated groups, whereas this was not the case for damage groups (Figure 5(f)). The infusion of iMVs-VCs promoted vascular reconstruction and regeneration.

iMVs-VCs possess capacities for migration, angiogenesis, and macrophage regulation

Angiogenesis is a dynamic process closely related to the migration of vascular cells.[26] To determine the migration of iMVs-VCs, we labeled iMVs-VCs by DiR and monitored them after local or systemic infusion by an in vivo imaging system (Figure 6(a)). In the IR model, the iMVs-VCs injected intravenously mainly migrated to the liver and kidney on day 1 after administration. Higher fluorescence intensity was detected at the IR-side kidney than on the normal side until day 3 (Figure 6(c)). In the skin wounds model, the iMVs-VCs locally injected around the subcutaneous skin wound were mainly located around the wound. Interestingly, a few Dir-labeled cells were also detected around the wound on the side which received only PBS injection (Figure 6(d)). The fluorescence signals were accumulated at the PBS side after 2 days of injection (Figure 6(e)), suggesting the chemotaxis of the iMVs-VCs to damaged tissues. To further clarify the location of the iMVs-VCs in damaged tissues, we marked the transplanted cells with human mitochondrial protein (MITO) for immunofluorescence staining of tissue sections. In the IR-side kidney, iMVs-VCs-derived ECs ($CD31^+MITO^+$) and pericytes ($CD140b^+MITO^+$) were detected around the microvessels. More iMVs-VCs were located around blood vessels of the IR kidney compared with the normal side (Figure 6(f)). Consistent with the biodistribution in the wound edges, the iMVs-VCs were aggregated around the blood vessels of the bilateral skin wounds (Figure 6(g)). The evidence indicated that the iMVs-VCs could migrate toward injured tissues and aggregate around the vessels to participate in repair.

To further study the destiny of the injected iMVs-VCs, we collected samples of kidney and skin treated with the iMVs-VCs on day 30 for immunofluorescence staining. A decrease in MITO-positive cells could be clearly observed. The transplanted ECs ($CD31^+$ $MITO^+$) and pericytes ($CD140b^+$ $MITO^+$) were directly involved in the vascular regeneration of damaged kidneys (Figure 7(a)), as well as in skin wounds (Figure 7(b)), suggesting high cell retention of iMVs-VCs in the ischemic and inflammatory conditions. Particularly, reconstructed vessels in healing skin exhibited significant perfusion. Notably, we could also observe a few $MITO^+$ cells on the normal side of the IR model, suggesting that iMVs-VCs were involved in the metabolism of normal blood vessels.

Endothelial cells have been reported to suppress the classical activation of macrophage (M1 phenotype) and promote alternative activation of macrophage (M2 phenotype), which may have anti-inflammatory and wound-healing effects.[27] To confirm whether iMVs-VCs could regulate macrophage subtypes, we examined the expression of CD68 (M1 phenotype marker) and CD163 (M2 phenotype marker) in post-IR kidneys and skin wounds. Immunofluorescence staining revealed that the accumulation of $CD68^+$ cells was increased in the IR group (Figure 8(a)) and skin damage model (Figure 8(c)). The infiltration of M1 macrophages was reduced by half after the infusion of iMVs-VCs (Figure 8(e) and (f)). In contrast, the accumulation of CD163-positive cells was tripled in the iMVs-VCs-treated IR model (Figure 8(e)). The increase was also statistically significant in the skin damage model (Figure 8(f)). The above results were further proved by GSEA analysis of gene expression in iMVs-VCs, which showed that iMVs-VCs expressed high levels of gene sets that positively regulate the activation of M2 phenotype (Figure 8(g)).

Taken together, these results indicate the iMVs-VCs could directly contribute to angiogenesis during tissue repair and attenuate the inflammatory response by regulating macrophage subtypes.

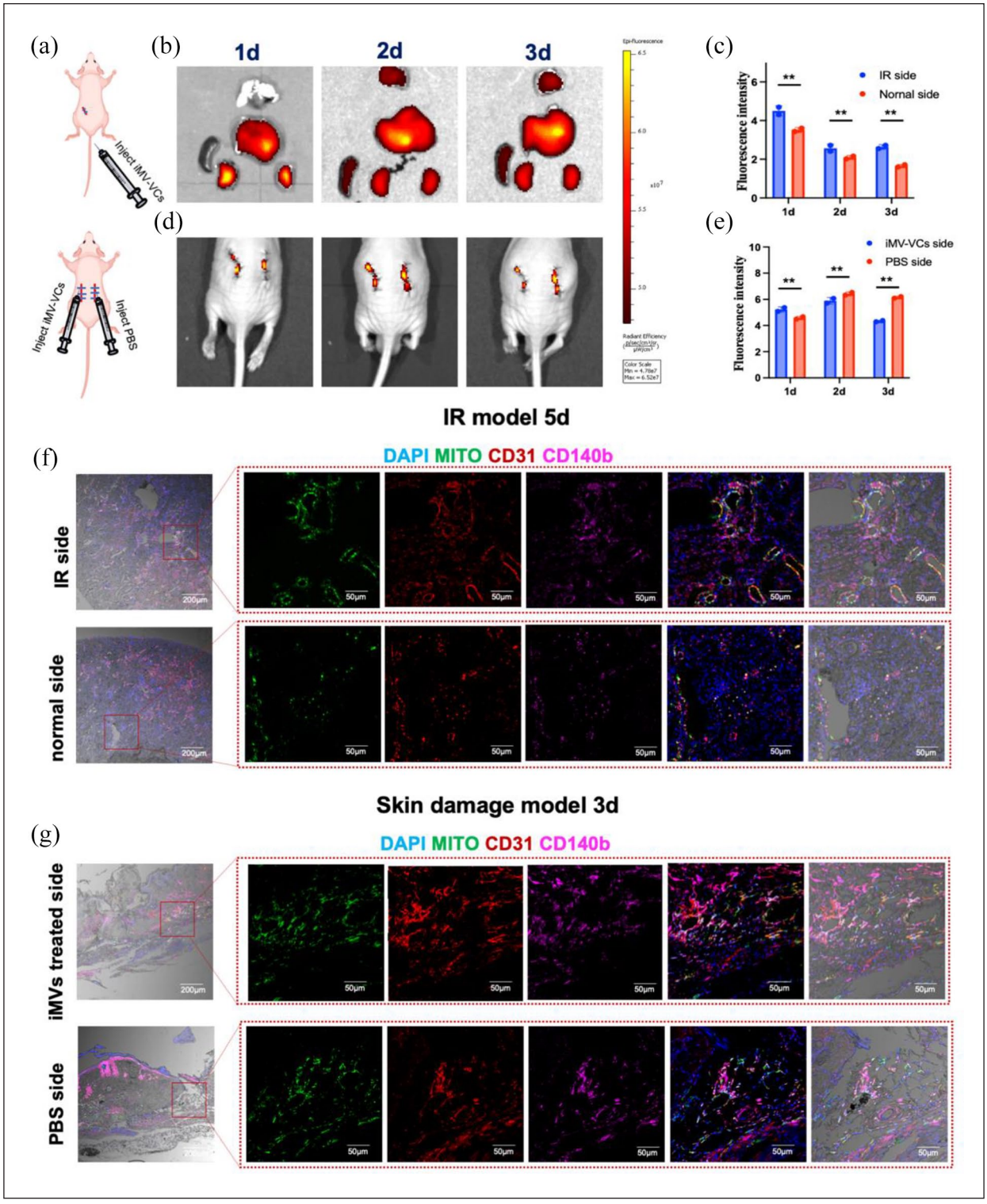

Figure 6. Migration of iMVs-VCs toward damaged tissues in vivo. (a) Experiment schematic. (b and c) After injecting labeled iMVs-VCs, the heart, lung, liver, spleen, and kidneys of mice were imaged to observe the biodistribution for the first 3 days. Fluorescence intensity was quantitated. Data are presented as the mean ± SD, $n = 2$/group, $^{*}p < 0.05$, $^{**}p < 0.01$. (d and e) The biodistribution of iMVs-VCs was observed in the skin damage model for the first 3 days. Quantitation of fluorescence intensity on bilateral skin. (f) Immunofluorescence for the distribution of iMVs-VCs in bilateral renal sections on day 5 after iMVs-VCs treatment. ECs derived from iMVs-VCs ($CD31^{+}$ and $Mito^{+}$), and pericytes derived from iMVs-VCs ($CD140b^{+}$ and $Mito^{+}$) were detected. (g) Immunofluorescence for the distribution of iMVs-VCs in bilateral skin sections on day 3 after treatment. Detection same as above. Scale bar, 200, 50 μm.

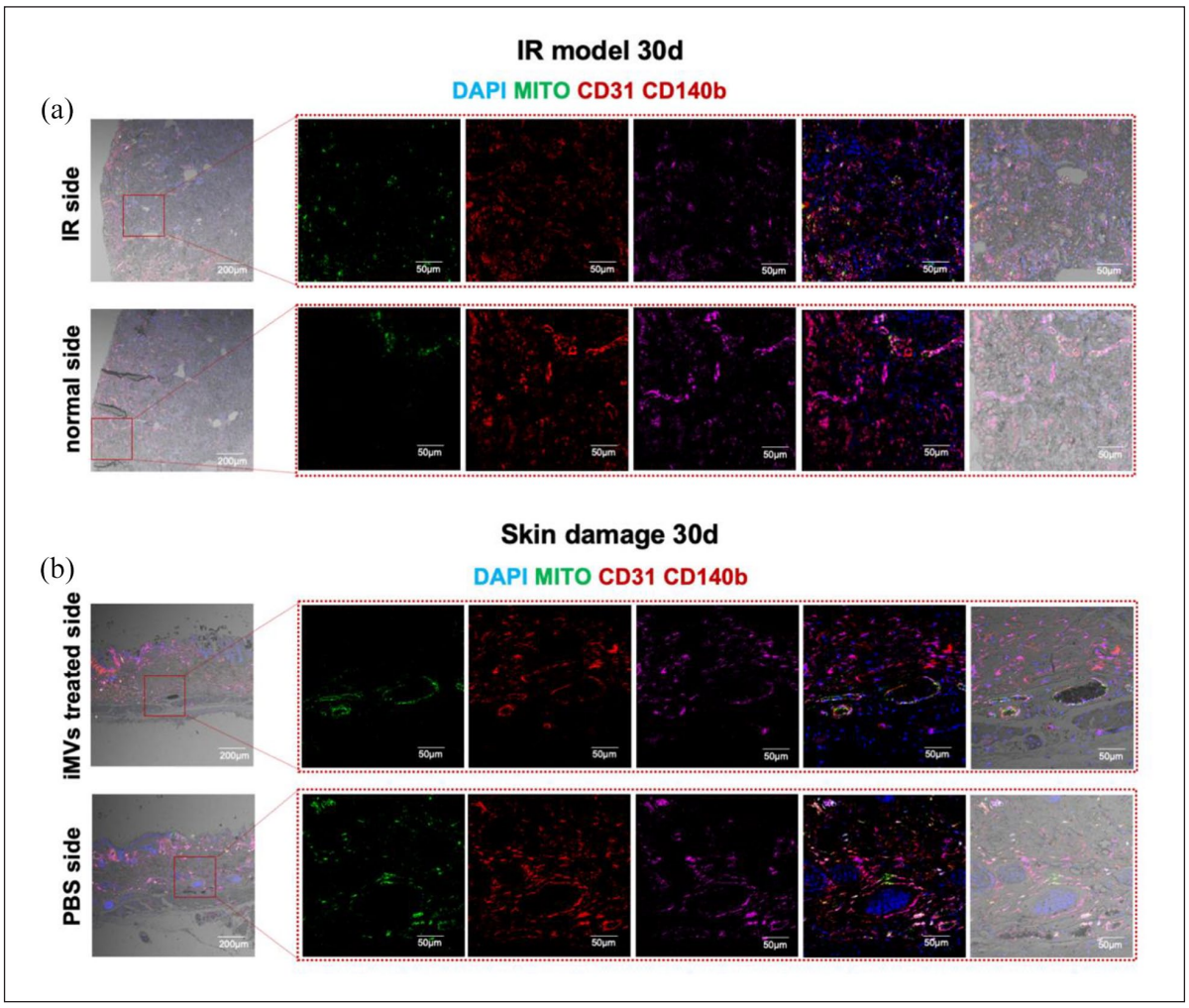

Figure 7. iMVs-VCs were involved in the revascularization of damaged tissues. (a) Immunofluorescence for the iMVs-VCs fate in bilateral kidneys of IR model on day 30. ECs derived from iMVs-VCs ($CD31^+$ and $Mito^+$), and pericytes derived from iMVs-VCs ($CD140b^+$ and $Mito^+$) were detected. (b) Immunofluorescence for the iMVs-VCs fate in bilateral skin on day 30. Detection same as above. Scale bar, 200, 50 μm.

The iMVs rapidly form perfused blood vessels in vivo

The above experiments confirmed that the cells derived from iMVs have a strong potential for angiogenesis. We then investigated whether the iMVs could be applied for angiogenesis and tissue regeneration. The ability of iMVs for angiogenesis in vivo was explored by subcutaneous transplantation into a custom-designed silicone tube. Fourteen days after transplantation, the histologic analysis showed that cells fully infiltrated the iMVs grafts, compared to the matrix-only group. Moreover, more perfused blood vessels formed in the iMVs group, especially in the areas close to the skin (Figure 9(a)). At 1 month of transplantation, the matrix group formed large volume cavities in the transplants. Cells and blood vessels were rarely observed on the distal side of the skin. Whereas, distinct blood vessels containing blood cells in the vessel lumen could be observed throughout the iMVs grafts (Figure 9(b)).

To clarify whether the formed vessels were derived from iMVs, STEM101 and CD31 were co-stained. Co-expressed vessels were observed at both time points. (Figure 9(c)). The results suggested that the transplantation of iMVs could rapidly form perfused blood vessels in vivo, which facilitated cell infiltration and tissue vascularization.

The iMVs promote muscle regeneration

Rapid angiogenesis is necessary to bring nutrients, immune cells, and oxygen to healing sites.[28] Skeletal muscle is highly vascularized with a dense microvasculature. An increase in angiogenesis can lead to the success of muscle regeneration.[29,30] The muscle injury model was established to investigate the effects of iMVs on muscle regeneration. 4 weeks after surgery, HE staining demonstrated that there was little evidence of cellular infiltration in collagen matrix grafts. Muscle defect with HUVECs implantation had a small amount of immature fibers formation near the

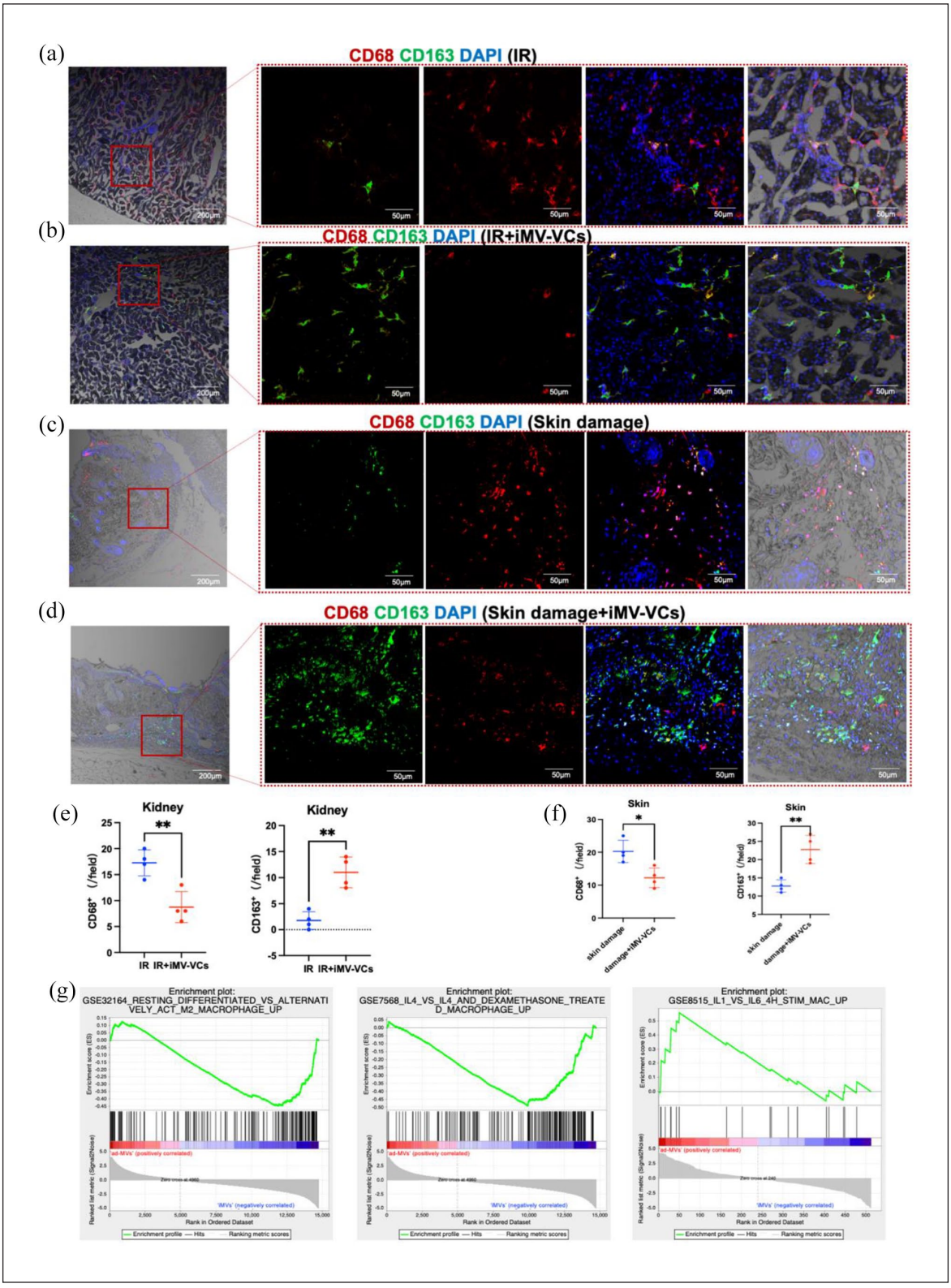

Figure 8. iMVs-VCs regulate macrophage subtypes in damaged tissues. (a and b) Immunofluorescence of CD68 and CD163 in the IR and iMVs-VCs treated groups on day 5 detected macrophage subtypes. CD68 in red as the M1 phenotype marker; CD163 in green as the M2 phenotype marker. Scale bar, 200, 50 μm. (c and d) Immunofluorescence of CD68 and CD163 in skin damage and iMVs-VCs treated groups on day 3. Scale bar, 200, 50 μm. (e and f) Quantification of CD68-positive cells and CD163-positive cells in tissue sections. Data are presented as the mean ± SD, $n = 4$/group, $^{*}p < 0.05$, $^{**}p < 0.01$. (g) GSEA analysis revealed that compared with ad-MVs, iMVs-VCs expressed more gene sets that positively regulate the activation of the M2 phenotype.

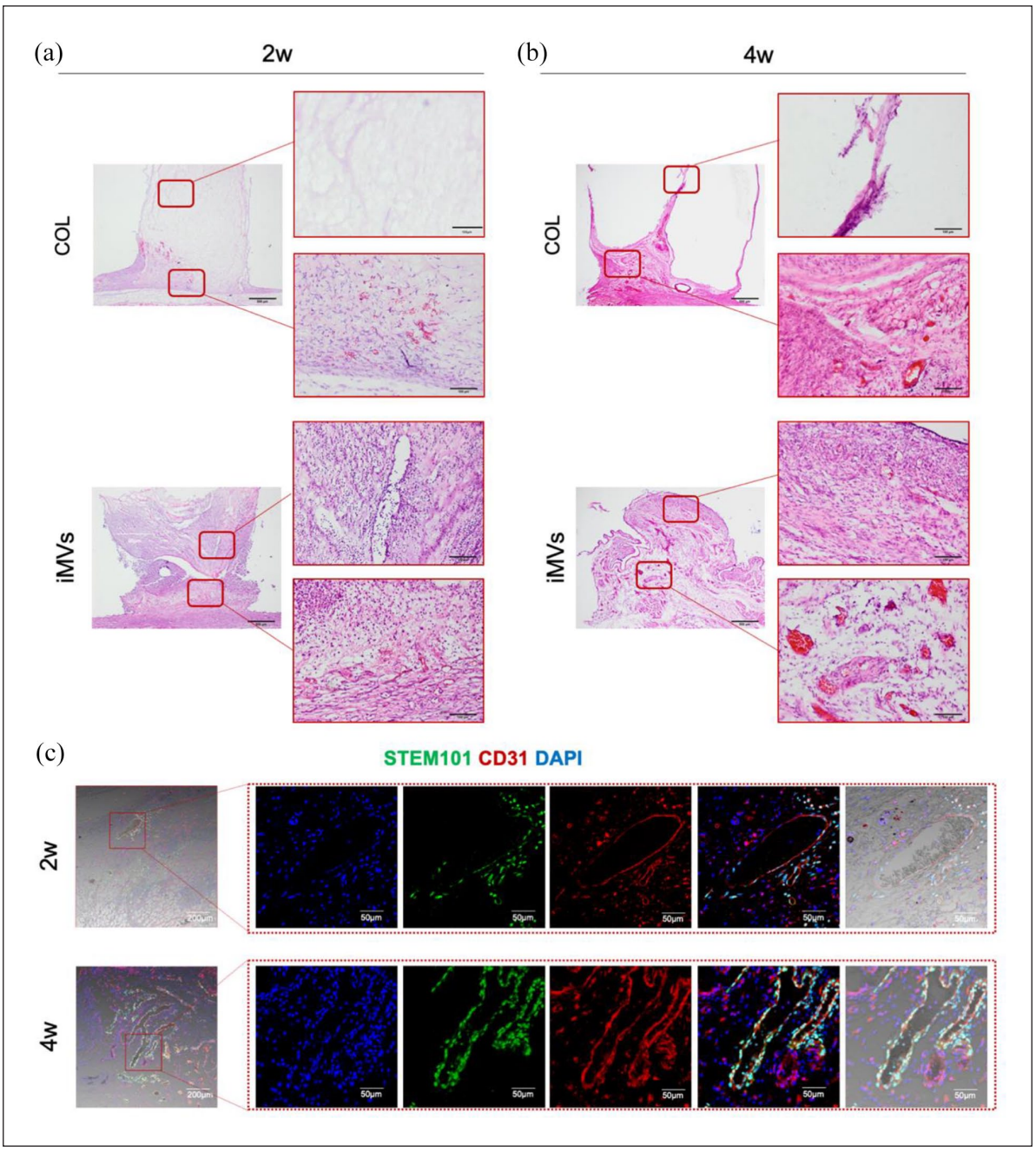

Figure 9. The angiogenic ability of iMVs in vivo. (a) HE staining was performed to reveal angiogenesis in different groups. Scale bar, 500, 50 μm. (b and c) Immunofluorescence of CD31 and STEM101 in iMVs group for illustration iMVs derived vessels. Scale bar, 200, 50 μm.

interface. Whereas, a notable presence of muscle fibers was clearly observed in the iMVs group (Figure 10(a)). Notably, perfused microvessels located in disordered myofibers were observed in the iMVs group. Regenerated myofibers were indicated by the presence of Myosin IIa (MF20) in defects.[6] The MF20 was rarely expressed in the collagen matrix group. Small amounts of MF20 were expressed at the edge of the defect in the group that received HUVECs transplantation, suggesting regeneration of myofibers. In the iMVs group, the ability to regenerate myofibers performed better with more notable expressions of MF20 (Figure 10(b)).

To explore whether muscle regeneration relied on angiogenesis, the microvessels were detected by the expression of CD31 in the defect sites. In the collagen matrix group, fewer blood vessels were formed than those in HUVECs and iMVs groups. Some of the microvessels co-expressed STEM101, representing that HUVECs and iMVs were involved in the angiogenic process in the defect area (Figure 10(c)). The results showed that the transplantation

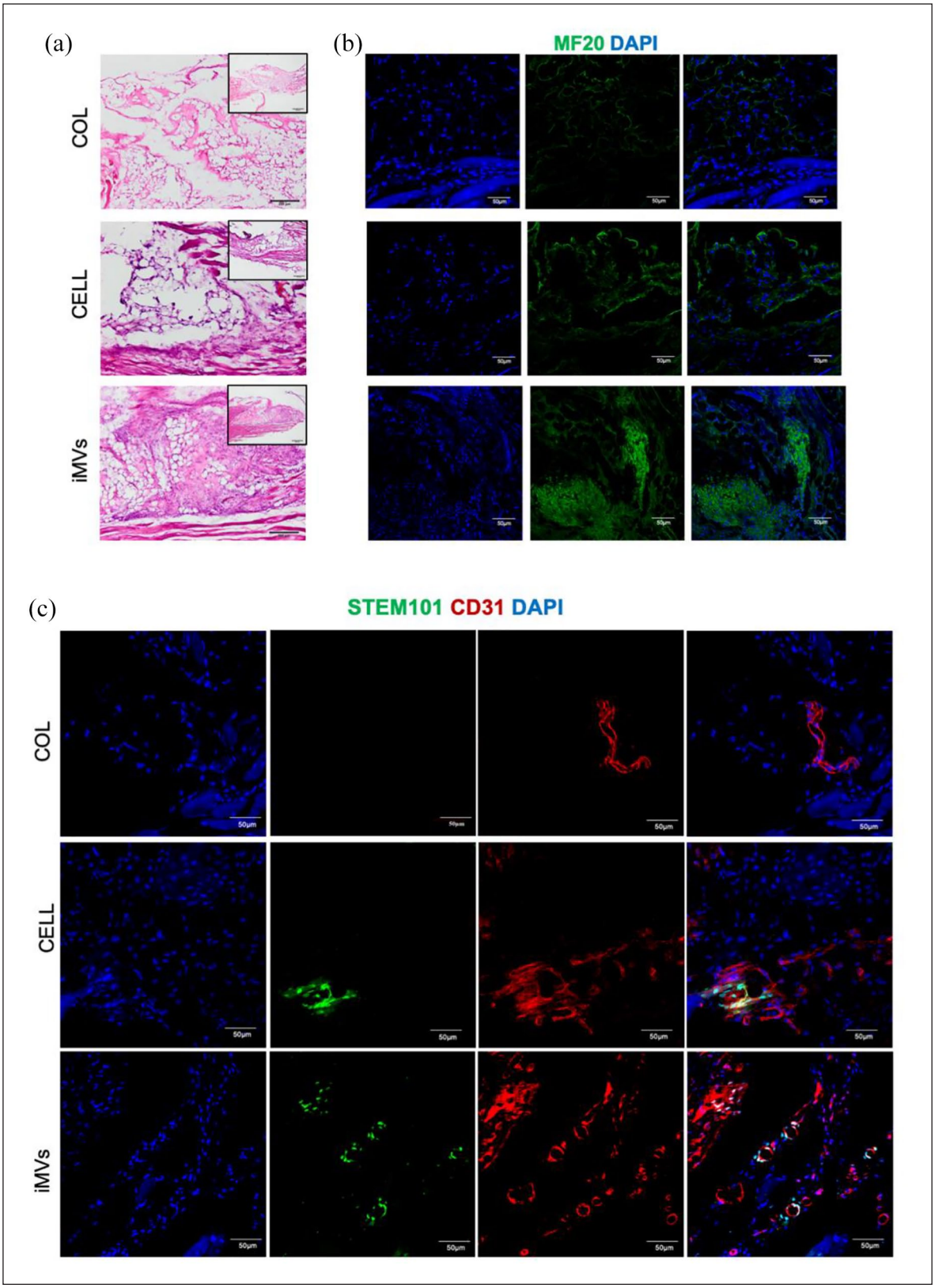

Figure 10. The effects of iMVs on muscle regeneration. (a-b) HE staining and Immunofluorescence analysis of MYH9 were performed to reveal the conditions of muscle regeneration. Scale bar, 200, 50 μm. (c) Immunofluorescence of CD31 and STEM101 in iMVs group for illustration iMVs derived vessels. Scale bar, 50 μm.

of iMVs increased the formation of blood vessels, which promoted the regeneration of muscles.

Transplantation of iMVs-VCs does not lead to tumor formation

Tumorigenesis by the undifferentiated pluripotent stem cells is a critical risk in the application of seed cells derived from iPSCs. To confirm whether the iMVs-VCs were tumorigenic, kidney samples of normal mice injected with iMVs-VCs were collected (Supplemental Figure S1(a)). There was no abnormal cell hyperplasia or oncogenesis in the renal according to HE and Masson staining (Supplemental Figure S1(b)). Moreover, the damaged skin with local injection of iMVs-VCs was collected on day 30 (Supplemental Figure S1(c)). The skin wound achieved full-thickness healing, and there was no tumor-like tissue formed after injection (Supplemental Figure S1(d)). Moreover, transplantation of iMVs in the subcutaneous and muscle of nude mice did not generate dysplastic tissue. Taken together, the results indicated that the iMVs-VCs were not tumorigenic.

Discussion

This study has revealed that the iMVs have similar gene expressions and structures to ad-MVs. the administration of the vascular cells derived from iMVs could rescue the renal ischemia-reperfusion and also promote earlier healing of skin wounds. In the early stages of tissue damage, the exogenous iMVs-VCs aggregate around blood vessels and attenuates the inflammation. The iMVs-VCs are directly involved in vascular reconstruction during late tissue repair. Furthermore, the transplantation of iMVs can form perfused blood vessels in the early period and promote muscle regeneration. These findings suggest that iMVs can be vascularization units for tissue repair and regeneration.

Several studies have demonstrated that microvessels isolated from the adipose tissue (ad-MVs) retained the native structure and cell composition of natural blood vessels.[5,31,32] Meanwhile, ad-MVs have the outstanding angiogenic potential of enhancing the vascularization of implants and grafts at defect sites.[7,12] However, the method of adipose tissue extraction is invasive, and its quantity is limited. In the present study, we explored the applications of hiPSCs-derived microvessels. Compared with microvessels derived from adipose tissue, hiPSCs have excellent proliferation capabilities, allowing for a large output of microvessels. The results revealed the similarities between iMVs and natural blood vessels and suggested promising prospects of iMVs for tissue regeneration. Moreover, we used iMVs-derived cells for the treatment of ischemic disease and also achieved good therapeutic effects. We provide not only a new vascularization strategy for tissue engineering but also a novel cell source for cell therapy.

hiPSCs can offer outstanding advantages in the treatment of disease because they can derive from patients' somatic cells, and have maximum immune compatibility.[33] Meanwhile, hiPSCs can differentiate into a sufficient number of various types of cells.[34] The microvessels derived from hiPSCs (iMVs) have been well established, and ECs, pericytes, and vSMCs can be efficiently differentiated from hiPSCs in one procedure, which is more practical than other protocols.[18] Especially in the present study, we first illustrated that the gene expressions of iMVs and ad-MVs are similar according to the results of RNA-seq. Moreover, the iMVs have a more prominent role in regulating endothelial cell migration and vascular differentiation, which is essential to angiogenesis.[35]

To explore the application potential of iMVs in vascularization strategy, different types of in vivo models were used. Ischemia/reperfusion contributes to increased mortalities during various pathological conditions such as stroke, kidney injury, and cardiac failure.[36] Cell therapy has achieved promising results. In our study, vascular cells derived from iMVs have been shown to have anti-inflammatory, anti-fibrotic, and pro-angiogenic therapeutic effects in the renal IR injury model. Moreover, local injection of iMVs-VCs could promote early healing of skin damage. The above results suggest that iMVs could be a new source of cells for the treatment of injury and ischemic diseases. The intact microvessels derived from adipose tissues have been applied to construct vascularized grafts due to their remarkable angiogenic activity.[37] Therefore, we investigated the angiogenic capacity of intact iMVs after transplantation. Subcutaneous transplantation and muscle defect models well demonstrated the potential of iMVs in tissue engineering.

Pericytes are the mural cell types that surround the endothelial layer to form integral functional vessels through interactive communication.[38] Previous studies have demonstrated that pericyte-endothelial cell attachment is essential in the vascular repair process.[39] In the tube formation assay of iMVs-VCs, pericytes aggregated around endothelial cells and formed complex networks. Furthermore, the iMVs-VCs still had a strong self-organization ability to reassemble after dissociation. Self-organization is not restricted to developmental processes. In adult organisms, tissue regeneration is also an emerging self-organizing feature of cells.[23] In the iMVs-VCs, tight cell-cell interactions could positively drive collective behaviors during the angiogenesis processes.[40]

Ischemia-reperfusion injury is a common complication of ischemic disease, which usually leads to further damage. In renal IR injury, pericytes play a central role in the development of interstitial fibrosis through differentiation into myofibroblasts.[41,42] However, some studies have revealed that pericytes therapy could improve vascularization and reduce interstitial fibrosis in a swine model of reperfused acute myocardial infarction.[43] In addition to its angiogenesis, the exogenous pericytes can ameliorate the

inflammation and attract circulating reparative cells to promote the healing process.[44] In the present study, we examined the effects of the iMVs-VCs on renal IR injury. Our data suggested that the iMVs-VCs could suppress the inflammatory response, which might attenuate renal fibrosis and preserve the functions.

One of the challenges of cell therapy is transplantation efficiency. Transplanted cells display a very high death percentage.[45,46] Many strategies have been used to enhance cell survival, including combined administration with supporting cells.[47] The results of biodistribution and IF showed considerable cell survival of the iMVs-VCs in vivo. Meanwhile, the iMVs-VCs could target the damaged tissues and aggregate around the blood vessels, which might be guided by a graded distribution of VEGF-A levels in a damaged environment.[48] During tissue repair, the iMVs-VCs were directly involved in the reconstruction of blood vessels. The regulation of the iMVs-VCs on the microenvironment might play a leading role in successful transplantation and restoration.

Adipose tissue-derived microvessels (ad-MVs) have served as natural vascularization units in angiogenesis research and tissue regeneration due to their outstanding ability to rapidly reassemble into microvascular networks.[37] The transplantation experiment showed that iMVs formed functional microvascular networks during the early period in our study. Our data also demonstrated the ability of iMVs to promote muscle regeneration by improving the vascularization of defect sites. Compared to ad-MVs, iMVs are derived from hiPSCs and can be massively induced, which is more promising for tissue engineering.

The present study provided a new source of cells for the treatment of ischemic diseases; besides preserving the functions after renal IR, the iMVs-VCs can promote earlier healing of skin wounds. We also found the administration of the iMVs-VCs could aggregate around blood vessels of damaged tissues and ameliorate the inflammation. In the process of tissue repair, the iMVs-VCs maintained a certain survival rate and participated in neovascularization. Moreover, iMVs could serve as a new kind of vascularization unit to promote tissue regeneration. However, there were still some limitations. Although we illustrated that the iMVs-VCs could attenuate the inflammation, more studies should be done to clarify the proteomics during the repair process. Besides, we should use more models to validate the application of iMVs in the future.

The field of regenerative medicine has been looking for a pluripotent stem cell able to be safely employed in therapy. The potential clinical applications of the hiPSCs have presented several problems, including genomic instability, and the risk of teratoma formation.[49] Highly efficient differentiation prior to cell transplantation is one way to eliminate the teratogenic potential of hiPSCs.[50] In the present study, we efficiently induced differentiation of hiPSCs toward the vascular lineage with no expressions of tumorigenic genes. No tumor-like tissue formed when iMV-derived vascular cells or intact iMVs were applied. However, further animal studies, including large animal models, to evaluate the safety and efficacy of iMVs are crucial before their translation into the clinic.

Conclusion

In the present study, we generated microvessels from pluripotent stem cells. The iMVs possess similar cell components and gene expression patterns to microvessels derived from adipose tissue. The cells derived from iMVs possess the capacities of migration, angiogenesis, and immune regulation, and could be directly involved in the regeneration of microvascular networks. The iMVs-VCs derived from microvessels could reduce renal injury after IR and promote skin wound healing. Besides, the transplantation of iMVs could form perfused blood vessels during the early period and promote tissue regeneration in a muscle damage model. Taken together, this study demonstrates that microvessels generated by iPSCs are a new source of microvessels for tissue repair and regeneration.

Author contribution

Xin Gao and Shixing Ma participated in the design of this study, and they both carried out the study and wrote the manuscript. Xiaotao Xing participated animal experiment and revised the manuscript. Jian Yang and Yejia Yu performed the statistical analysis. Xun Xu and Cheng Liang collected important background information. Lei Liu, Li Liao, and Weidong Tian carried out the design, data acquisition, and manuscript editing. All authors gave final approval and agree to be accountable for all aspects of the work.

Declaration of conflicting interests

The author(s) declared no potential conflicts of interest with respect to the research, authorship, and/or publication of this article.

Funding

The author(s) disclosed receipt of the following financial support for the research, authorship, and/or publication of this article: This work was supported by grants from the National Key Research and Development Program of China (2021YFA1100603), the National Natural Science Foundation of China (82071092, U21A20369), and the Fundamental Research Funds for the Central Universities (YJ201878).

ORCID iD

Li Liao https://orcid.org/0000-0002-1937-9212

Supplemental material

Supplemental material for this article is available online.

References

1. Ding MH, Lozoya EG, Rico RN, et al. The role of angiogenesis-inducing microRNAs in vascular tissue engineering. *Tissue Eng Part A* 2020; 26(23-24): 1283–1302.

2. Linn T, Schmitz J, Hauck-Schmalenberger I, et al. Ischaemia is linked to inflammation and induction of angiogenesis in pancreatic islets. *Clin Exp Immunol* 2006; 144(2): 179–187.
3. Roux BM, Cheng MH and Brey EM. Engineering clinically relevant volumes of vascularized bone. *J Cell Mol Med* 2015; 19(5): 903–914.
4. Santos MI and Reis RL. Vascularization in bone tissue engineering: physiology, current strategies, major hurdles and future challenges. *Macromol Biosci* 2010; 10(1): 12–27.
5. Aghazadeh Y, Poon F, Sarangi F, et al. Microvessels support engraftment and functionality of human islets and hESC-derived pancreatic progenitors in diabetes models. *Cell Stem Cell* 2021; 28(11): 1936–1949.e8.
6. Pilia M, McDaniel J, Guda T, et al. Transplantation and perfusion of microvascular fragments in a rodent model of volumetric muscle loss injury. *Eur Cell Mater* 2014; 28: 11–24.
7. Xu X, Liang C, Gao X, et al. Adipose tissue-derived microvascular fragments as vascularization units for dental pulp regeneration. *J Endod* 2021; 47(7): 1092–1100.
8. Sun X, Wu J, Qiang B, et al. Transplanted microvessels improve pluripotent stem cell-derived cardiomyocyte engraftment and cardiac function after infarction in rats. *Sci Transl Med* 2020; 12(562): eng1015050861946.
9. Song HG, Rumma RT, Ozaki CK, et al. Vascular tissue engineering: progress, challenges, and clinical promise. *Cell Stem Cell* 2018; 22(3): 340–354.
10. Rickel AP, Deng X, Engebretson D, et al. Electrospun nanofiber scaffold for vascular tissue engineering. *Mater Sci Eng C Mater Biol Appl* 2021; 129: 112373.
11. Saberianpour S, Heidarzadeh M, Geranmayeh MH, et al. Tissue engineering strategies for the induction of angiogenesis using biomaterials. *J Biol Eng* 2018; 12: 36.
12. Kamat P, Frueh FS, McLuckie M, et al. Adipose tissue and the vascularization of biomaterials: stem cells, microvascular fragments and nanofat-a review. *Cytotherapy* 2020; 22(8): 400–411.
13. Chen SG, Ugwu F, Li WC, et al. Vascular tissue engineering: advanced techniques and gene editing in stem cells for graft generation. *Tissue Eng Part B Rev* 2021; 27(1): 14–28.
14. Orlova VV, van den Hil FE, Petrus-Reurer S, et al. Generation, expansion and functional analysis of endothelial cells and pericytes derived from human pluripotent stem cells. *Nat Protoc* 2014; 9(6): 1514–1531.
15. Cheung C, Bernardo AS, Trotter MW, et al. Generation of human vascular smooth muscle subtypes provides insight into embryological origin-dependent disease susceptibility. *Nat Biotechnol* 2012; 30(2): 165–173.
16. Patsch C, Challet-Meylan L, Thoma EC, et al. Generation of vascular endothelial and smooth muscle cells from human pluripotent stem cells. *Nat Cell Biol* 2015; 17(8): 994–1003.
17. Wimmer RA, Leopoldi A, Aichinger M, et al. Human blood vessel organoids as a model of diabetic vasculopathy. *Nature* 2019; 565(7740): 505–510.
18. Wimmer RA, Leopoldi A, Aichinger M, et al. Generation of blood vessel organoids from human pluripotent stem cells. *Nat Protoc* 2019; 14(11): 3082–3100.
19. Frueh FS, Später T, Scheuer C, et al. Isolation of murine adipose tissue-derived microvascular fragments as vascularization units for tissue engineering. *J Vis Exp* 2017; (122): eng1013132521940.
20. Ozbilgin S, Ozkardesler S, Akan M, et al. Renal ischemia/reperfusion injury in diabetic rats: the role of local ischemic preconditioning. *Biomed Res Int* 2016; 2016: 8580475.
21. McCoy MG, Seo BR, Choi S, et al. Collagen I hydrogel microstructure and composition conjointly regulate vascular network formation. *Acta Biomater* 2016; 44: 200–208.
22. Wolint P, Bopp A, Woloszyk A, et al. Cellular self-assembly into 3D microtissues enhances the angiogenic activity and functional neovascularization capacity of human cardiopoietic stem cells. *Angiogenesis* 2019; 22(1): 37–52.
23. Xavier da Silveira Dos Santos A and Liberali P. From single cells to tissue self-organization. *FEBS J* 2019; 286(8): 1495–1513.
24. Herrler T, Wang H, Tischer A, et al. Decompression of inflammatory edema along with endothelial cell therapy expedites regeneration after renal ischemia-reperfusion injury. *Cell Transplant* 2013; 22(11): 2091–2103.
25. Ishihara J, Ishihara A, Starke RD, et al. The heparin binding domain of von Willebrand factor binds to growth factors and promotes angiogenesis in wound healing. *Blood* 2019; 133(24): 2559–2569.
26. Lee HW, Xu Y, He L, et al. Role of venous endothelial cells in developmental and pathologic angiogenesis. *Circulation* 2021; 144(16): 1308–1322.
27. Chawla A, Nguyen KD and Goh YP. Macrophage-mediated inflammation in metabolic disease. *Nat Rev Immunol* 2011; 11(11): 738–749.
28. DiPietro LA. Angiogenesis and wound repair: when enough is enough. *J Leukoc Biol* 2016; 100(5): 979–984.
29. Reddy LVK, Murugan D, Mullick M, et al. Recent approaches for angiogenesis in search of successful tissue engineering and regeneration. *Curr Stem Cell Res Ther* 2020; 15(2): 111–134.
30. Latroche C, Weiss-Gayet M, Muller L, et al. Coupling between myogenesis and angiogenesis during skeletal muscle regeneration is stimulated by restorative macrophages. *Stem Cell Reports* 2017; 9(6): 2018–2033.
31. Strobel HA, Gerton T and Hoying JB. Vascularized adipocyte organoid model using isolated human microvessel fragments. *Biofabrication* 2021; 13(3): eng1015219641758.
32. Acosta FM, Stojkova K, Brey EM, et al. A straightforward approach to engineer vascularized adipose tissue using microvascular fragments. *Tissue Eng Part A* 2020; 26(15–16): 905–914.
33. Yamanaka S. Pluripotent stem cell-based cell therapy-promise and challenges. *Cell Stem Cell* 2020; 27(4): 523–531.
34. Picanço-Castro V, Moreira LF, Kashima S, et al. Can pluripotent stem cells be used in cell-based therapy? *Cell Reprogram* 2014; 16(2): 98–107.
35. Lamalice L, Le Boeuf F and Huot J. Endothelial cell migration during angiogenesis. *Circ Res* 2007; 100(6): 782–794.
36. Shiva N, Sharma N, Kulkarni YA, et al. Renal ischemia/reperfusion injury: an insight on in vitro and in vivo models. *Life Sci* 2020; 256: 117860.
37. Laschke MW, Später T and Menger MD. Microvascular fragments: more than just natural vascularization units. *Trends Biotechnol* 2021; 39(1): 24–33.
38. Liu C, Ge HM, Liu BH, et al. Targeting pericyte-endothelial cell crosstalk by circular RNA-cPWWP2A inhibition aggravates diabetes-induced microvascular dysfunction. *Proc Natl Acad Sci U S A* 2019; 116(15): 7455–7464.

39. Wang M, Xu H, Li Y, et al. Exogenous bone marrow derived-putative endothelial progenitor cells attenuate ischemia reperfusion-induced vascular injury and renal fibrosis in mice dependent on pericytes. *Theranostics* 2020; 10(26): 12144–12157.
40. Wong SP, Rowley JE, Redpath AN, et al. Pericytes, mesenchymal stem cells and their contributions to tissue repair. *Pharmacol Ther* 2015; 151: 107–120.
41. Castellano G, Franzin R, Stasi A, et al. Complement activation during ischemia/reperfusion injury induces pericyte-to-myofibroblast transdifferentiation regulating peritubular capillary lumen reduction through pERK signaling. *Front Immunol* 2018; 9: 1002.
42. Chou YH, Pan SY, Shao YH, et al. Methylation in pericytes after acute injury promotes chronic kidney disease. *J Clin Investig* 2020; 130(9): 4845–4857.
43. Ellison-Hughes GM and Madeddu P. Exploring pericyte and cardiac stem cell secretome unveils new tactics for drug discovery. *Pharmacol Ther* 2017; 171: 1–12.
44. Avolio E, Meloni M, Spencer HL, et al. Combined intramyocardial delivery of human pericytes and cardiac stem cells additively improves the healing of mouse infarcted hearts through stimulation of vascular and muscular repair. *Circ Res* 2015; 116(10): e81–e94.
45. Abdelwahid E, Kalvelyte A, Stulpinas A, et al. Stem cell death and survival in heart regeneration and repair. *Apoptosis* 2016; 21(3): 252–268.
46. Geng YJ. Molecular mechanisms for cardiovascular stem cell apoptosis and growth in the hearts with atherosclerotic coronary disease and ischemic heart failure. *Ann N Y Acad Sci* 2003; 1010: 687–697.
47. Recchia FA and Sharp TE. Combination cell therapy for ischemic cardiomyopathy: is the whole greater than sum of its parts? *J Am Coll Cardiol* 2017; 70(20): 2516–2518.
48. Gerhardt H and Betsholtz C. How do endothelial cells orientate? *EXS* 2005; (94): 3–15.
49. Suman S, Domingues A, Ratajczak J, et al. Potential clinical applications of stem cells in regenerative medicine. *Adv Exp Med Biol* 2019; 1201: 1–22.
50. Gorecka J, Kostiuk V, Fereydooni A, et al. The potential and limitations of induced pluripotent stem cells to achieve wound healing. *Stem Cell Res Ther* 2019; 10(1): 87.